

GENERAL ARTICLE

SPECC1L regulates palate development downstream of IRF6

Everett G. Hall^{1,†}, Luke W. Wenger¹, Nathan R. Wilson^{1,‡}, Sraavya S. Undurty-Akella², Jennifer Standley², Eno-Abasi Augustine-Akpan³, Youssef A. Kousa^{4,§}, Diana S. Acevedo¹, Jeremy P. Goering¹, Lenore Pitstick⁵, Nagato Natsume⁶, Shahnawaz M. Paroya¹, Tamara D. Busch², Masaaki Ito⁶, Akihiro Mori⁶, Hideto Imura⁶, Laura E. Schultz-Rogers⁷, Eric W. Klee^{7,8}, Dusica Babovic-Vuksanovic⁸, Sarah A. Kroc⁸, Wasiu L. Adeyemo⁹, Mekonen A. Eshete¹⁰, Bryan C. Bjork⁵, Satoshi Suzuki^{2,6}, Jeffrey C. Murray², Brian C. Schutte^{11,12}, Azeez Butali³ and Irfan Saadi^{1,*}

¹Department of Anatomy and Cell Biology, University of Kansas Medical Center, Kansas City, KS 66160, USA,

²Department of Pediatrics, Craniofacial Anomalies Research Center, University of Iowa, Iowa City, IA 52242,

USA, ³Department of Oral Pathology, Radiology and Medicine/Dow Institute for Dental Research, College of

Dentistry, University of Iowa, Iowa City, IA 52242, USA, ⁴Department of Biochemistry and Molecular Biology,

Michigan State University, East Lansing, MI 48824, USA, ⁵Department of Biochemistry, Midwestern University,

Downers Grove, IL 60515, USA, ⁶Division of Research and Treatment for Oral and Maxillofacial Congenital

Anomalies, Aichi Gakuin University Hospital, 2-11 Suemori-Dori, Nagoya, Chikusa-ku, Japan, ⁷Center for

Individualized Medicine, Mayo Clinic, Rochester, MN 55905, USA, ⁸Department of Clinical Genomics, Mayo

Clinic, Rochester, MN 55905, USA, ⁹Department of Oral and Maxillofacial Surgery, College of Medicine,

University of Lagos, Lagos, PMB 12003, Nigeria, ¹⁰Department of Plastic and Reconstructive Surgery, Addis

Ababa University, Addis Ababa, PO Box 26493, Ethiopia, ¹¹Department of Microbiology and Molecular Genetics,

Michigan State University, East Lansing, MI 48824, USA and ¹²Department of Pediatrics and Human

Development, Michigan State University, East Lansing, MI 48824, USA

*To whom correspondence should be addressed at: Department of Anatomy and Cell Biology, University of Kansas Medical Center, Kansas City, KS 66160, USA. Tel: +1 9135887667; Fax: +1 9135885677; Email: isaadi@kumc.edu

Abstract

SPECC1L mutations have been identified in patients with rare atypical orofacial clefts and with syndromic cleft lip and/or palate (CL/P). These mutations cluster in the second coiled-coil and calponin homology domains of SPECC1L and severely affect the ability of SPECC1L to associate with microtubules. We previously showed that gene-trap knockout of *Specc1l* in

[†]Clinical Research Training Center, Institute of Clinical and Translational Sciences, Washington University, St. Louis, MO, USA.

[‡]Center for Regenerative Medicine, Massachusetts General Hospital, Harvard Medical School, Boston, MA, USA.

[§]Division of Neurology, Children's National Health System, Washington, DC, USA.

Received: April 23, 2019. Revised: December 13, 2019. Accepted: January 2, 2020

mouse results in early embryonic lethality. We now present a truncation mutant mouse allele, *Specc1*^{ΔCS10}, that results in perinatal lethality. *Specc1*^{ΔCS10/ΔCS10} homozygotes showed abnormal palate rugae but did not show cleft palate. However, when crossed with a gene-trap allele, *Specc1*^{trGT/ΔCS10} compound heterozygotes showed a palate elevation delay with incompletely penetrant cleft palate. *Specc1*^{trGT/ΔCS10} embryos exhibit transient oral epithelial adhesions at E13.5, which may delay shelf elevation. Consistent with oral adhesions, we show periderm layer abnormalities, including ectopic apical expression of adherens junction markers, similar to *Irf6* hypomorphic mutants and *Arhgap29* heterozygotes. Indeed, SPECC1L expression is drastically reduced in *Irf6* mutant palatal shelves. Finally, we wanted to determine if SPECC1L deficiency also contributed to non-syndromic (ns) CL/P. We sequenced 62 Caucasian, 89 Filipino, 90 Ethiopian, 90 Nigerian and 95 Japanese patients with nsCL/P and identified three rare coding variants (p.Ala86Thr, p.Met91Iso and p.Arg546Gln) in six individuals. These variants reside outside of SPECC1L coiled-coil domains and result in milder functional defects than variants associated with syndromic clefting. Together, our data indicate that palate elevation is sensitive to deficiency of SPECC1L dosage and function and that SPECC1L cytoskeletal protein functions downstream of IRF6 in palatogenesis.

Introduction

Orofacial clefting is the most common craniofacial congenital malformation, with an incidence of ~1 in 800 live-births (1,2). Among orofacial clefts, ~70% of cases manifest as isolated or non-syndromic cleft lip with or without cleft palate (nsCL/P) (3), while the remaining 30% consists of >275 different syndromic forms of clefting (4).

The underlying pathology of many syndromic CL/P cases can be narrowed down to a single causative gene and shows a Mendelian inheritance pattern in affected families. In contrast, nsCL/P often presents in families with incomplete penetrance and represents a complex disorder with a heterogeneous genetic component (1,5–7). Genome-wide association studies in conjunction with traditional candidate gene and linkage analyses have contributed to the identification of several nsCL/P-associated genes (8–10). One method of conceptualizing the effect of these many genes is by organizing them into regulatory networks. For instance, both IRF6 and GRHL3 mutations have been identified in patients with Van der Woude syndrome (VWS) (11–14). Common variants in these two genes also increase the risk for CL/P in cases with isolated CL/P (15–20). Previous studies have shown that IRF6 regulates GRHL3 expression (21,22), and mouse mutants for the two genes show similar phenotypes (14,23,24). Together, these studies implicate functional deficiency of an IRF6-GRHL3 network in nsCL/P (12,17,18). This network has been expanded to include ARHGAP29 (25–28).

The IRF6-GRHL3 network is required for specification and proper differentiation of the periderm (14,22,29); a single layer of specialized epithelial cells that prevents abnormal epithelial adhesions during embryonic development (30). The periderm achieves this non-adhesive property by localizing adhesion molecules away from its apical surface, preventing cell–cell adhesion (29,30). During palatogenesis, the periderm is selectively removed at the medial edge epithelium to allow palatal shelves to adhere at E14.5 (31). Deficiencies in the IRF6-GRHL3 network result in an absent or abnormal periderm layer. *Irf6* mutants lack periderm and result in ectopic permanent adhesions all over the body, including the oral cavity, which causes cleft palate (23,24). Heterozygotes for *Irf6*^{R84C} and *Irf6*^{gt} alleles, as well as heterozygotes for an *Arhgap29* null allele, show transient oral adhesions (23,24,32). These transient oral adhesions frequently accompany a delay in palatal shelf elevation at E14.5 (32). Considering that rare and common variants in IRF6 have been associated with nsCL/P (15,19,20), IRF6 regulation of the periderm represents a critical pathway in palatogenesis. Identification of additional members of this pathway is necessary to further elucidate nsCL/P etiology.

We first identified SPECC1L mutations in two patients with atypical clefts (33). At the time, we posited that atypical clefts are a severe manifestation of more common cleft lip and palate phenotype. Thus, we proposed that pathogenetic mechanisms underlying SPECC1L deficiency would also result in more common syndromic and nsCL/P. Consistent with our proposition, 10 additional SPECC1L mutations were identified in a total of 31 patients originally diagnosed with clefting-associated autosomal dominant Opitz G/BBB (OMIM #145410) and Teebi hypertelorism syndromes (OMIM #145420) (34–36). Bhoj et al. (34) compiled a relatively distinct phenotypic profile of patients with SPECC1L mutations that includes hypertelorism, orofacial clefting, wide short nose with large tip and ventral body wall closure defects (omphalocele). This range of malformations led them to propose an independent autosomal dominant SPECC1L mutation syndrome. Interestingly, these syndromic mutations cluster in either the second coiled-coil or the calponin homology domains of SPECC1L.

To validate that a decrease in SPECC1L dosage or function can affect midface development, we generated gene-trap and truncation *Specc1* mutant mouse alleles. Indeed, compound heterozygotes with a gene-trap and a truncation allele exhibit a delay in palate elevation. Furthermore, we identify defects in the periderm of *Specc1* compound heterozygous embryos and show that SPECC1L expression in the palate requires IRF6. We also sequenced 426 individuals with nsCL/P from five different populations and identified three rare SPECC1L variants. A total of six individuals (1.4%) were heterozygous for one of these three variants. Functional analyses indicate that these variants result in partial loss of function. These studies show that deficiency of SPECC1L is sufficient to disrupt palate development and implicate SPECC1L in the expanding IRF6-GRHL3 orofacial clefting gene network.

Results

Moderate reduction of *Specc1* in mouse results in palate elevation defect

We previously reported that severe deficiency of *Specc1* using gene-trap constructs results in early embryonic lethality by embryonic day E9.5 (37). These mutants exhibited an open neural tube and defects in cranial neural crest cell delamination from the anterior neural folds. While a deficiency in neural crest cell function is a plausible cause of a craniofacial defect (38,39), early embryonic lethality prevented confirmation of a direct role for SPECC1L in midface or palate development. Therefore, we sought to generate alternative *Specc1*-deficient alleles that would allow embryos to survive longer in gestation to study these perinatal

phenotypes. We utilized zinc finger nuclease (ZFN)-based genomic deletions to target the 3' end of exon 4, which yielded a 154 bp deletion (Fig. 1A). Sequencing of reverse transcription polymerase chain reaction (RT-PCR) product revealed that the deletion abolished the exon 4 splice donor site (Fig. 1A), resulting in the use of a cryptic splice site within intron 4 and the subsequent introduction of a novel coding sequence (Fig. 1B). This novel sequence coded for nine amino acids followed by a stop codon, leading to premature truncation of the protein (Fig. 1C). For clarity, we have termed this allele *Specc1l*^{ΔC510}, as it results in the loss of the 510 amino acids at the C-terminal end of the protein (Fig. 1C). To validate this truncation, we performed western blot analysis with an antibody targeting the N-terminal end of SPECC1L. Indeed, a band can be seen at ~100 kDa in the mutant, compared to wild-type (WT) SPECC1L at ~150 kDa (Fig. 1D; right). In contrast to the embryonic lethality seen in gene-trap homozygotes, *Specc1l*^{ΔC510/ΔC510} mutants showed perinatal lethality (Fig. 1D). Examination of mutant pups immediately after birth revealed a gasping behavior followed by death within 24 h. Potential causes of this respiratory distress including esophageal adhesions (23,24), autonomic nervous system and neuromuscular defects (40) are under investigation. *Specc1l*^{ΔC510/ΔC510} homozygotes showed no gross malformations, apart from occasional size differences and curly tail phenotypes (Fig. 1D; arrow). Additionally, we did not detect instances of cleft palate at E18.5 on the C57BL6/J background (N = 6). However, when we looked at palate rugae, we observed patterning defects and poorly developed or missing rugae 7 and 7b (Supplementary Material, Fig. S1, A vs. D).

We hypothesized that a further reduction in *Specc1l* dosage by crossing gene-trap and truncation alleles would result in palate defects. To achieve this, we utilized a newly generated gene-trap allele, termed *Specc1l*^{cGT-ko} (abbreviated *Specc1l*^{cGT} from here on) using a multifunctional gene-trap cassette adapted for targeted trapping (Fig. 1A) (41,42). Homozygous *Specc1l*^{cGT/cGT} mutants undergo embryonic lethality at E9.5 (Fig. 1E), consistent with our previous gene-trap alleles, *Specc1l*^{RRH048} and *Specc1l*^{DTM096} (37). Interestingly, *Specc1l*^{cGT/cGT} homozygotes often show complete neural tube closure failure (Fig. 1E; arrows), while *Specc1l*^{RRH048} and *Specc1l*^{DTM096} mutants only show closure defects in the cranial neural tube (37). This is indicative of an increased trapping efficiency of the *Specc1l*^{cGT} allele. Consistently, western blot analysis of lysates from *Specc1l*^{cGT/cGT} mutant E8.5 embryos showed almost no observable WT SPECC1L (Fig. 1E).

To evaluate the impact of *Specc1l*^{cGT/ΔC510} compound heterozygosity on palate development, we harvested embryos at E13.5–E15.5. Compared to control embryos (Fig. 2A, C and E), *Specc1l*^{cGT/ΔC510} mutants (Fig. 2B, D, F and G) appeared smaller and manifested subepidermal blebbing at E13.5 (Fig. 2B; arrowheads), and at E14.5 (Fig. 2D; arrowheads). This blebbing resolved by E15.5, except in occasional cases of hemorrhaging (Fig. 2F and G; arrowheads). Importantly, ~57% (n = 14) of *Specc1l*^{cGT/ΔC510} mutants showed vertically oriented (unelevated) palatal shelves when compared to littermate controls at E14.5 (Fig. 2D, arrows; P < 0.0004, Fisher Exact Test). This delayed palate elevation was also observed in *Specc1l*^{DTM096/ΔC510} compound heterozygotes, albeit at only ~40% (n = 5) (Supplementary Material, Fig. S2). Consistently, western blot analysis of *Specc1l*^{cGT/ΔC510} embryo tissue showed lower WT SPECC1L level than that in *Specc1l*^{DTM096/ΔC510} mutant tissue (Supplementary Material, Fig. S2). The palate elevation defect persists in ~8% of *Specc1l*^{cGT/ΔC510} mutants at E15.5 and later (n = 12), resulting in cleft palate (Fig. 2G; arrows).

Given that the elevation defect we identified resolves in most embryos by E15.5, and we wanted to confirm a palate-specific defect in these compound mutants. We argued that if this was a simple delay in overall development, the palate would eventually develop normally. So, we closely examined closed mutant palates of E18.5 embryos and observed that all mutants had discontinuous patterning and missing rugae when compared to controls (Supplementary Material, Fig. S1), showing that even when these mutants recover from a delay in elevation, palate development is still disrupted. Furthermore, cell proliferation levels were also unchanged in mutant palatal shelves relative to WT (Supplementary Material, Fig. S3). Together, these results demonstrate that reduced *Specc1l* dosage is sufficient to specifically disrupt palate development.

Specc1l^{cGT/ΔC510} mutants show ectopic oral adhesions and abnormal periderm

A delay in palatal shelf elevation is also found in other mouse models (43–45). Most notably, *Arhgap29* heterozygotes showed a palate elevation delay (32), accompanied by ectopic transient oral adhesions. Therefore, we histologically scanned the oral cavity of our mutants. Indeed, our *Specc1l* compound mutants showed several occurrences of ectopic adhesions (Fig. 3). Evidence of oral adhesions was found in the anterior nasal cavity (Fig. 3A vs. B), the palate hinge region (Fig. 3C vs. D) and between palatal shelf and buccal or lingual epithelia (Fig. 3E vs. F). These oral adhesions almost always accompanied a dissociation of epithelia from the underlying mesenchyme in paraffin sections (Fig. 3A' vs. B', C' vs. D' and E' vs. F').

Specc1l^{cGT/ΔC510} mutants show abnormal adherens junction staining in the periderm

To investigate how SPECC1L deficiency in our compound mutants could cause both a delay in palatal shelf elevation and transient oral adhesions, we first evaluated SPECC1L expression in the palate by co-staining cranial E13.5 and E14.5 sections for SPECC1L and ΔNp63, a marker for the basal epithelium (Fig. 4A–C and A'–C'). Indeed, we found that SPECC1L is expressed in the cranial neural crest derived palatal mesenchyme (Fig. 4A–C and A'–C'), as well as both the ΔNp63-positive basal cells (Fig. 4A') and ΔNp63-negative periderm cells of the palatal shelf (Fig. 4A'; arrow).

Previous studies have shown that ectopic oral adhesions involve abnormalities of the periderm (46). *Irf6* mouse mutants exhibit a complete absence of periderm cells (29), resulting in severe oral adhesions and permanent cleft palate (23,24). However, partial loss of IRF6 function has been shown to result in the mislocalization of adherens junction markers to the apical surface of the periderm, which is normally devoid of cell adhesion molecules (29,30). IRF6 deficiency also results in increased actin stress fiber formation (47). Similarly, we previously showed increased actin filament and adherens junction marker staining upon SPECC1L deficiency (33,37). Therefore, we examined these markers in the oral periderm of our compound mutants. Co-staining for ΔNp63 and β-catenin (Fig. 4D–K) revealed abnormal apical expression of membrane-associated β-catenin in mutant periderm (Fig. 4G vs. K; arrows). Manual scoring of cells along the buccal and lingual palatal shelf interfaces revealed a significantly greater number of abnormal periderm cells in compound mutant sections (20/386 cells) compared to WT (4/365 cells),

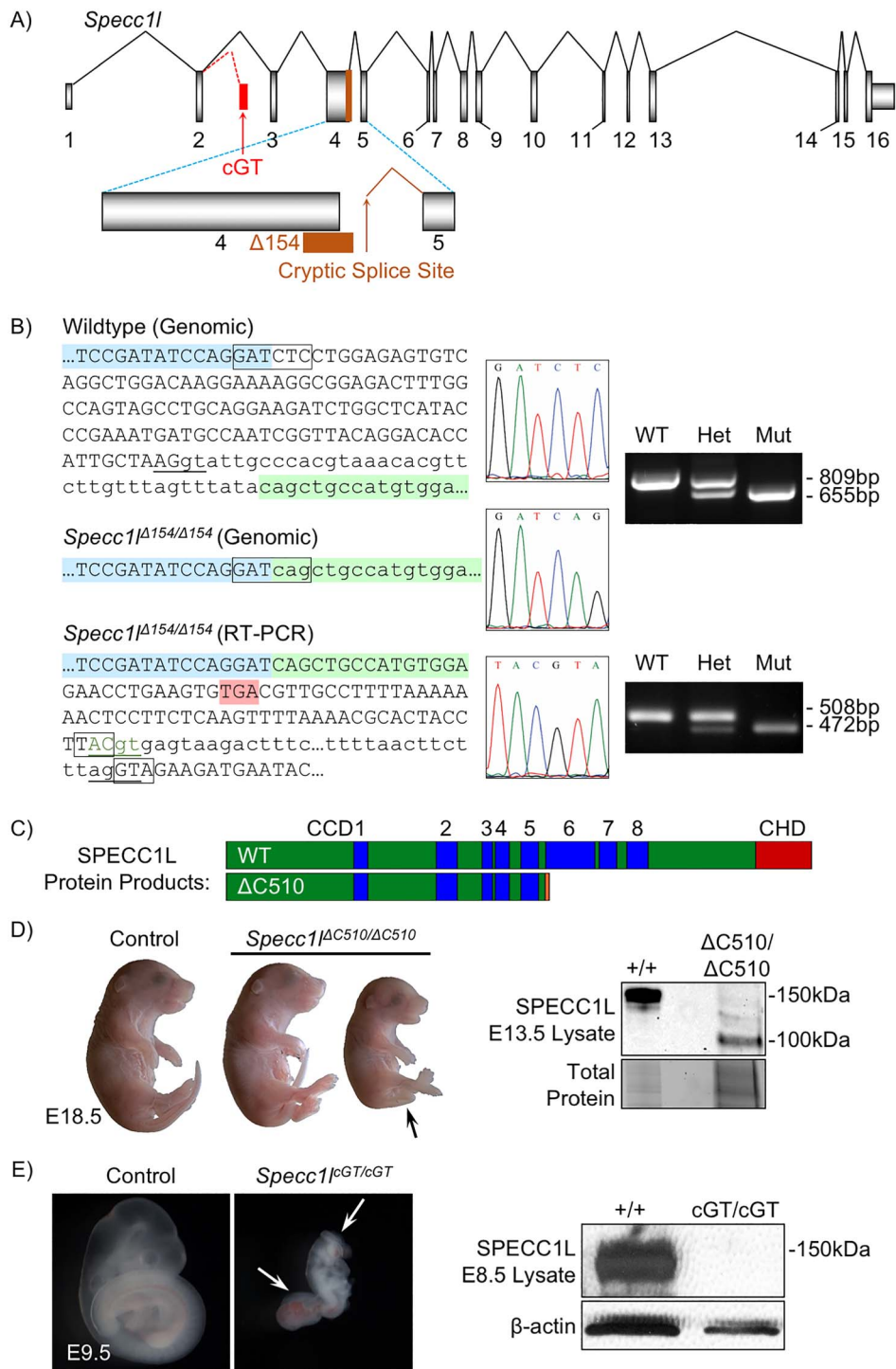


Figure 1. Generation of truncation *Specc1l* allele. (A) Schematic of *Specc1l* introns and exons depicting the locations of the cGT construct (red) and zinc finger nuclease (ZFN) deletion $\Delta 154$ (orange). (B) $\Delta 154$ ZFN deletion removes the canonical splice donor of exon 4, resulting in the usage of cryptic splice donor within intron 4 (RT-PCR; underlined green sequence) and subsequent truncation of the protein due to the introduction of a stop codon (RT-PCR; red highlighting). Genotyping by PCR amplification of genomic DNA and RT-PCR reveals a size difference between WT and $\Delta 154$ bands. (C) Diagram of WT and $\Delta C510$ SPECC1L protein. Orange section represents the nine novel amino acids. (D) *Specc1* ^{$\Delta C510/\Delta C510$} embryos die shortly after birth and are occasionally smaller than wild-type (WT) littermates. Western blotting shows a ~50 kDa size decrease in $\Delta C510$ homozygotes compared to WT control lysates. (E) *Specc1*^{cGT/cGT} embryos exhibit embryonic lethality with open neural folds (arrows) at E9.5, compared to littermate control. Western blotting shows a loss of SPECC1L protein in cGT homozygotes compared to WT control lysates.

consistent with the occurrence of transient oral adhesions ($P < 0.001$; Fisher Exact Test).

We also stained for filamentous actin (F-actin) using phalloidin and found a generally increased staining in mutant palate

epithelium and mesenchyme with regions of disorganized filaments (Fig. 4L-S; arrows). This increase in staining was less pronounced than the changes seen in gene-trap homozygotes (37) but more pronounced than in *Specc1* ^{$\Delta C510/\Delta C510$} mutants

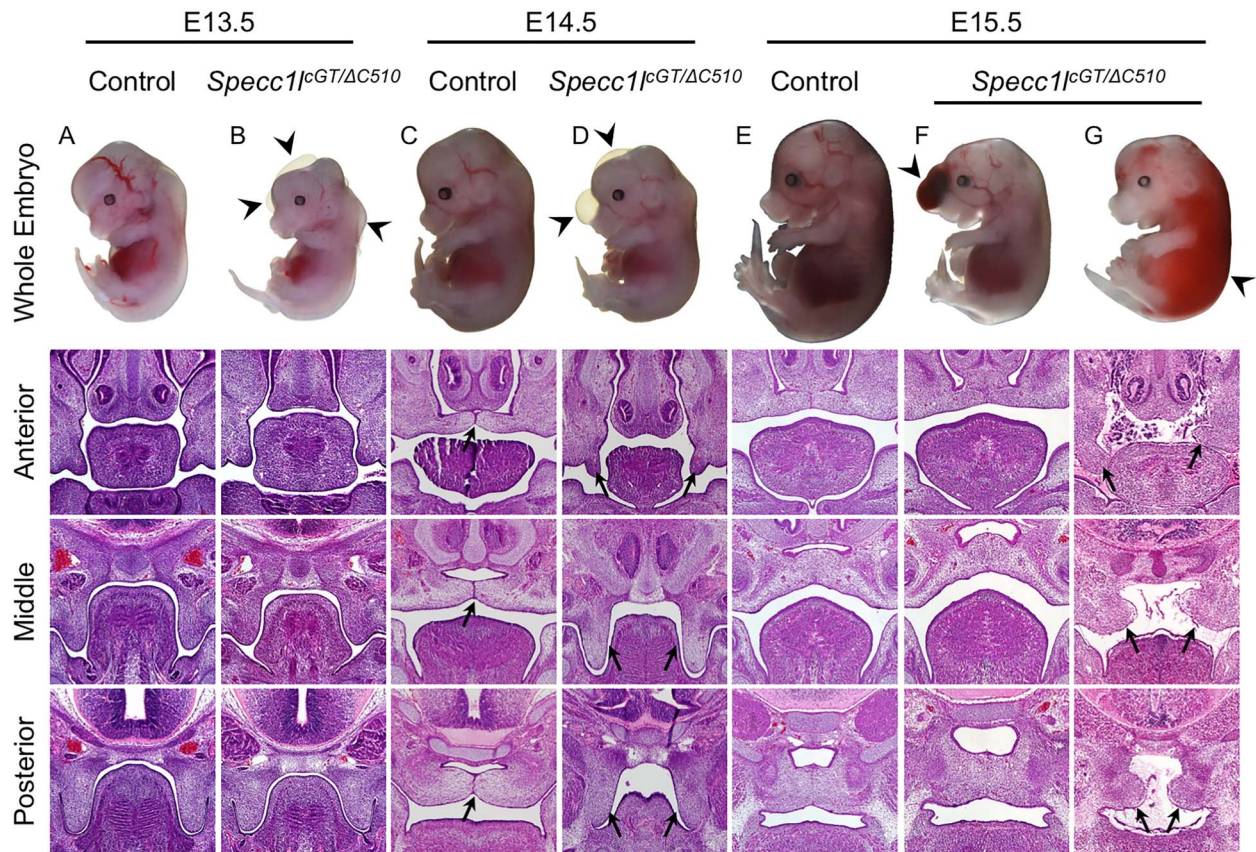


Figure 2. *Specc1*^{cGT/ΔC510} compound mutants exhibit palatal shelf elevation delay. (A–G) Representative whole mount images (top row) and coronal H&E palate sections (bottom three rows) of control and *Specc1*^{cGT/ΔC510} embryos from E13.5 to E15.5. Compound mutants show edema, midline subepidermal blebbing (B and D; arrowheads) and occasional hemorrhaging (F and G; arrowheads) compared to control embryos. At E14.5, ~66% of mutant embryos had palatal shelves that had not elevated (D; arrows) compared to littermate controls (C; arrows). By E15.5, most mutants had closed palates (F), indicating that these mutants experience a delay in palatal shelf elevation. However, cleft palate can occur in mutant embryos with severe phenotypes (G; arrows).

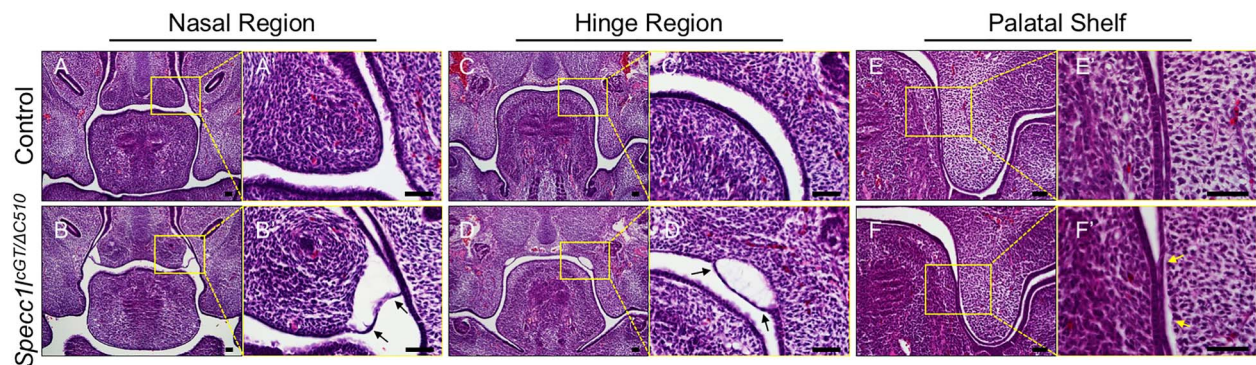


Figure 3. *Specc1*^{cGT/ΔC510} compound mutants show transient oral adhesions. (A–F) Coronal H&E palate sections of WT and *Specc1*^{cGT/ΔC510} mutant embryos at E13.5. Compound mutants show evidence of adhesions between the oral and nasal cavity epithelia (A vs. B; arrows) and between the oral and tongue epithelia (C vs. D; arrows). Adhesions were also identified at the junction between the tongue and palatal shelf (E vs. F; arrows), which resulted in separation of the palatal shelf epithelium from the mesenchyme (F'; arrows). Scale bars are 50 μm.

(Supplementary Material, Fig. S4), supporting a dosage dependent effect of *SPECC1L* levels on F-actin. Together, these results indicate that both adherens junction markers and F-actin within the palate epithelial cells are sensitive to reduced *Specc1* dosage and present abnormal expression of adhesion markers as a potential mechanism for oral adhesions in our compound mutants.

SPECC1L expression in the palate is dependent on IRF6 transcription factor

The similar adhesions and molecular changes in *Irf6* and *Arhgap29* heterozygotes and our *Specc1* mutants suggest that *SPECC1L* regulation of the periderm may functionally overlap with the IRF6 pathway. To test if *SPECC1L* could be connected to

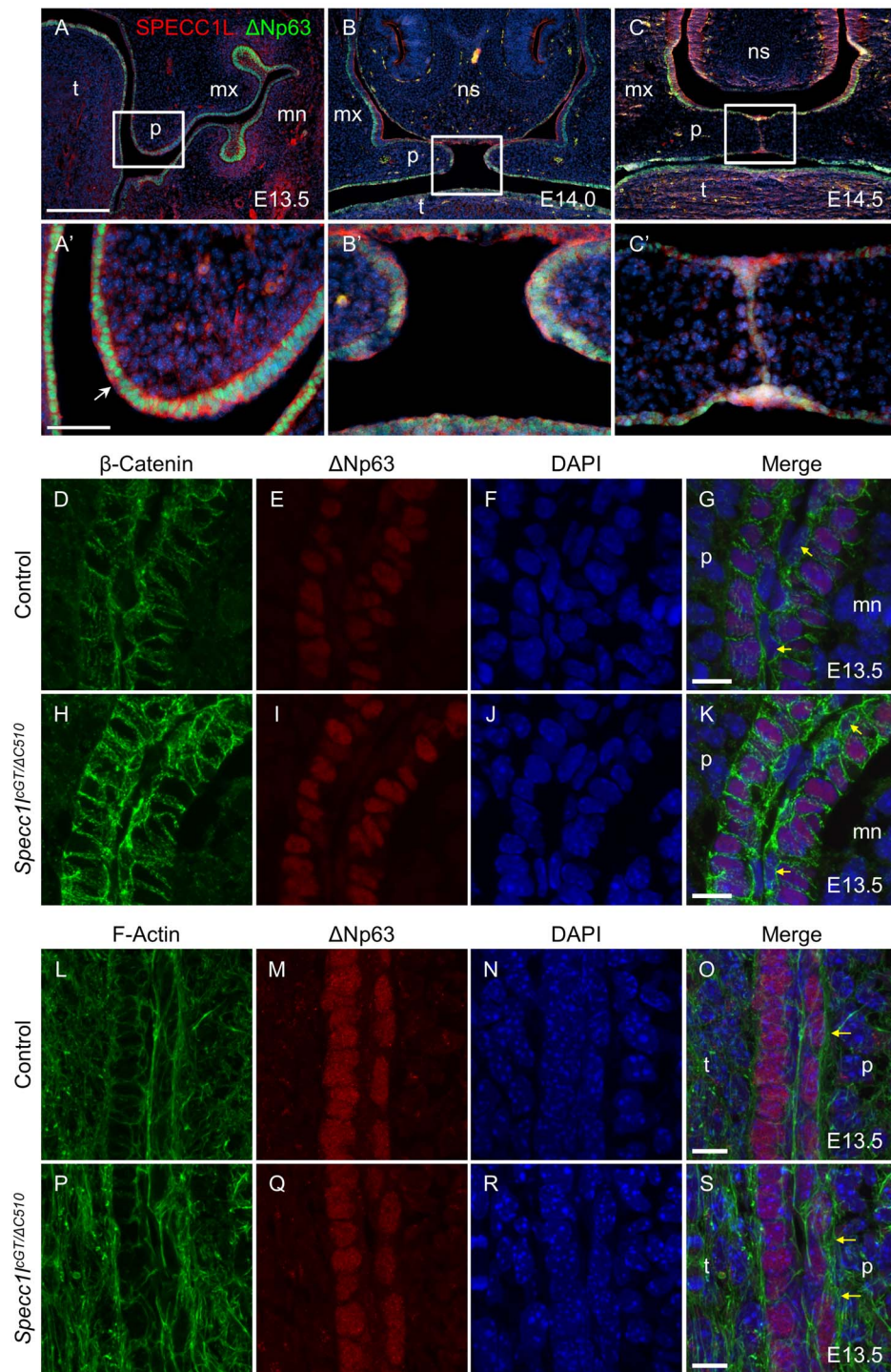


Figure 4. Periderm of *Specc1*^{CGT/ΔC510} embryos show changes in F-actin and adherens junction markers consistent with abnormal adhesion. (A–C) Immunostaining for SPECC1L (red) and ΔNp63 (green; basal epithelial marker) on coronal sections between E13.5 and E14.5. SPECC1L expression is present in the periderm and basal layers of the epithelium (A'; arrow), as well as the underlying mesenchyme (A–C). Scale bar for A–C is 2 mm and for A'–C' is 50 μm. (D–K) Coronal sections of E13.5 WT and *Specc1*^{CGT/ΔC510} palatal shelf epithelia co-immunostained for cell junction marker β-catenin (D and H) and basal epithelium marker ΔNp63 (E and I). Both WT and mutant sections contain flattened, ΔNp63-negative periderm cells (G and K; arrows). However, the mutant sections have abnormal apical β-catenin staining on some periderm cells (G vs. K; arrows). (L–S) Sections stained with phalloidin (L and P) show increased F-actin staining in the mutants compared to controls (O vs. S). Scale bars are 10 μm. p, palatal shelf; mx, maxillary process; mn, mandibular process; t, tongue; ns, nasal septum.

the IRF6 regulatory pathway, we looked at SPECC1L expression in the palate of *Irf6* knockout embryos (*Irf6*^{-/-}) (23). Indeed, SPECC1L expression was reduced in the epithelium of the *Irf6*^{-/-} palatal shelves (Fig. 5A vs. B). It was previously shown that K14

promoter-based transgenic expression of *Irf6* in the oral epithelia (*Tg*^{K14-Irf6/+}) partially rescued the oral adhesion phenotype in *Irf6* knockout mice (48). Consistent with this rescue, SPECC1L expression was restored in the oral epithelium of *Irf6*^{-/-};

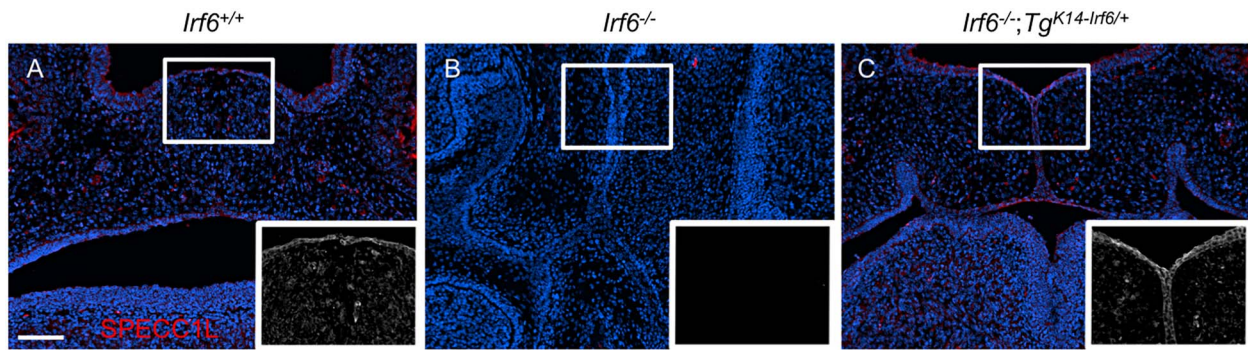


Figure 5. IRF6 is required for SPECC1L expression in the palate. Immunostaining of coronal embryonic palate sections at E15.5. (A) SPECC1L is expressed widely (red) in the palate in WT mice. (B) *Irf6* null mice exhibit abnormal oral adhesions throughout the oral cavity and loss of SPECC1L expression. (C) These phenotypes are rescued with transgenic expression of *Irf6* in the oral ectoderm using a Keratin 14 promoter. Grayscale insets are of red channel. Scale bar is 100 μm .

Tg^{K14-Irf6/+} embryos (Fig. 5B vs. C). Furthermore, IRF6 expression was not altered in our *Specc1L^{IGT/ΔCS10}* mutants (Supplementary Material, Fig. S5). Together, these results show that SPECC1L expression in the palatal shelves requires IRF6 function.

Identification of non-synonymous SPECC1L coding variants in nsCL/P patients

Given that SPECC1L mutations were identified in patients with atypical and syndromic CL/P (33–36), we posited that variants might also contribute to nsCL/P. To test this, we sequenced the coding region of SPECC1L (NM_015330.5; NP_056145.4) in 426 nsCL/P patient samples. These included 62 samples from Iowa Caucasians, 89 from the Philippines, 90 from Ethiopia, 90 from Nigeria and 95 samples from Japan (Fig. 6). One novel (c.273G>A, p.Met91Iso), two rare (c.256G>A, p.Ala86Thr; c.1637G>A, p.Arg546Gln), and one population specific (895A>G, p.Thr299Ala) variant were identified. The variants p.Met91Iso, p.Arg546Gln and p.Thr299Ala were identified once each in the Filipino, Iowa Caucasian and Japanese samples, respectively. The p.Met91Iso variant was not present in either ExAC or gnomAD databases ($n=372\,576$) (49). The p.Arg546Gln variant was not present in the ExAC database ($n=121\,096$), but was present in six individuals in the gnomAD samples ($n=282\,708$; allele frequency = 0.0000025). The p.Thr299Ala variant (rs146907080) was encountered a combined 88 times only in East Asian samples of the ExAC and gnomAD databases ($n=28\,606$; allele frequency = 0.00308), indicating that it is an East Asian population-specific variant. Interestingly, the p.Ala86Thr novel variant was identified in four different Japanese individuals with nsCL/P ($n=95$; allele frequency = 0.021) compared to 0/8654 and 1/18394 occurrence in East Asian samples in ExAC and gnomAD databases ($n=27\,048$; allele frequency = 0.000037). To determine if p.Ala86Thr was perhaps a Japanese population-specific common variant, we looked closely into gnomAD database (152 Japanese alleles) as well as into TogoVar database containing 3.5k Japanese exome data (3.5k_JPN, 7104 alleles) and extensive Japanese SNP data (JGA-SNP, 364 306 alleles) (50). We did not find any occurrence of p.Ala86Thr among any of these Japanese alleles. In contrast, the p.Thr299Ala East Asian variant was identified in 2/152 (~1%) gnomAD Japanese alleles, 75/7104 (~1%) 3.5k_JPN alleles and 3729/364306 (~1%) SNP-JGA alleles, as expected. These data suggest enrichment of p.Ala86Thr variant in Japanese CL/P samples.

Enrichment of SPECC1L variants in nsCL/P is predicated upon these variants being inherited with incomplete penetrance or working in conjunction with other variants not yet described.

We did not have parental samples to determine whether these variants—particularly p.Ala86Thr in four Japanese individuals—occurred *de novo* or were inherited with incomplete penetrance of the CL/P phenotype. However, we have identified the p.Arg546Gln variant in another patient with classic features associated with syndromic SPECC1L variants, including hypertelorism and CL/P (34). This is the first instance of a SPECC1L variant outside of second coiled-coil or calponin homology domains manifesting syndromic anomalies. This individual inherited the p.Arg546Gln variant paternally, and the father does not manifest any overt phenotypes. This finding is consistent with our hypothesis that these rare SPECC1L variants are not *de novo*, but enriched in individuals with CL/P. Interestingly, this syndromic individual with p.Arg546Gln variant also carried a *de novo* 14q22.3 microduplication, involving the OTX2 and TMEM260 genes. According to DECIPHER (decipher.sanger.ac.uk) and DGV (<http://dgv.tcag.ca>), OTX2 ($n=4$; DECIPHER 288272, DGV nsv1048136) or TMEM260 ($n=2$; DECIPHER 288575) microduplications do not show any craniofacial phenotypes. Larger duplications involving OTX2 and 5–6 downstream genes have been identified in individuals with micrognathia ($n=1$; DECIPHER 328344) or hemifacial microsomia ($n=1$) (51). Therefore, the SPECC1L R546Q variant, in combination with this microduplication or as yet unknown genetic or environmental perturbation, may underlie the syndromic manifestation in this patient. These results are consistent with the hypothesis that SPECC1L variants with subtle effects on SPECC1L function, in combination with other genetic/environmental insults, lead to CL/P.

Expression analysis of SPECC1L variants shows reduced acetylation of SPECC1L-associated microtubules

The identification of one novel and two very rare variants suggested that they may affect SPECC1L function. None of these variants lie in any of the coiled-coil domains of SPECC1L protein, in contrast with previously identified SPECC1L mutations in patients with atypical facial clefts (33), autosomal-dominant Opitz G/BBB syndrome (36) and Teebi hypertelorism syndrome (34,35). Thus, we hypothesized that these variants from nsCL/P patients will affect SPECC1L function to a different or lesser degree than those identified in syndromic patients.

We previously analyzed pathogenic SPECC1L variants identified in syndromic patients in a qualitative overexpression assay, wherein a SPECC1L-GFP fusion construct was transfected into U2OS osteosarcoma cells, followed by examination of the cells 24 h after transfection (33,36). In brief, we found that overexpressed WT SPECC1L-GFP strongly associated with a subset

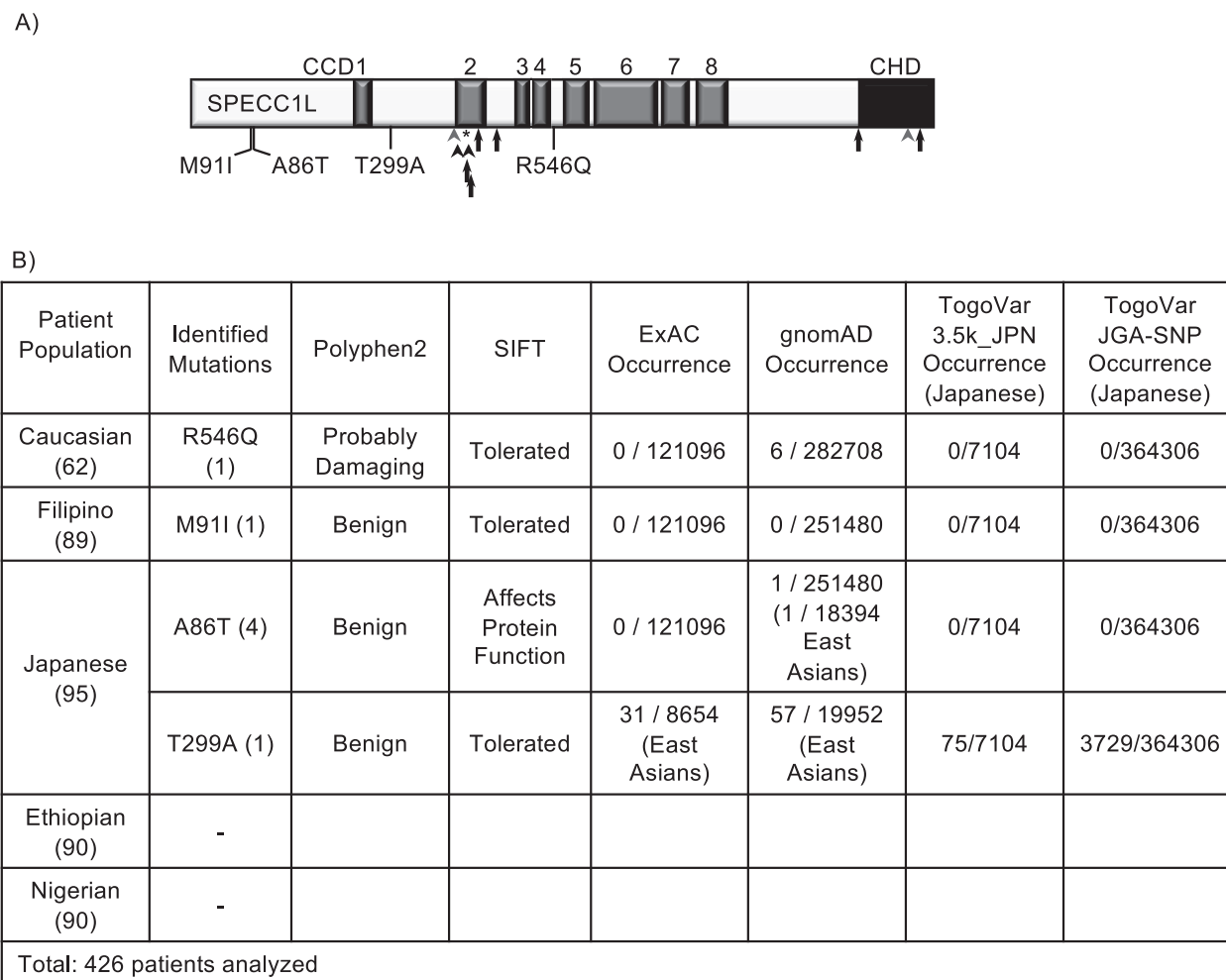


Figure 6. SPECC1L variants in patients with non-syndromic orofacial clefting. (A) Schematic representation of SPECC1L protein showing positions of the eight coiled-coil domains (CCD; gray), calponin homology domain (CHD; black), as well as the heterozygous mutations identified in patients with non-syndromic cleft lip/palate (A86T, M91I, T299A, R546Q). Also shown are the previously identified mutations found in a patient with Oblique Facial Clefts [Saadi et al., (33); asterisk], two multigenerational families with autosomal dominant Opitz G/BBB syndrome [Kruszka et al. (36); gray arrowheads], patients with Teebi hypertelorism syndrome [Bhoj et al. (35); black arrowheads], and the additional syndromic patients identified in [Bhoj et al., (34); black arrows]. (B) Chart describing the source of the patient samples that were sequenced this analysis including the patient population, the incidence of each variant within that population, Polyphen2 and SIFT substitution predictions, and occurrence in ExAC, gnomAD and TogoVar databases (49,50,63,64).

of microtubules in an elaborate ectopic pattern. We also showed that this subset of microtubules is heavily acetylated (33,36). In contrast, introduction of syndromic SPECC1L variants (33,36) resulted in severely disrupted microtubule association and acetylation. We utilized this disruption as a readout to evaluate the impact of our non-syndromic SPECC1L variants.

Compared to WT SPECC1L-GFP, none of the four variants showed any demonstrable differences in the ability to associate with microtubules after 24 h of transfection (not shown). To sensitize the assay, we first removed the C-terminal GFP tag to prevent any ectopic microtubule association or aggregation that may be mediated by the tag itself, and instead used anti-SPECC1L antibody to detect transfected cells (Fig. 7; Supplementary Material, Fig. S6). We also added an 8 h time-point following transfection and co-stained for acetylated microtubules. We found that even without the GFP tag, WT SPECC1L associated with a subset of microtubules that formed an elaborate cytoplasmic pattern within almost 80% of transfected cells (Fig. 7A and D). Only a small fraction of cells showed an incomplete microtubule pattern, which may represent cells

where the elaborate pattern is not yet developed. As expected, a syndromic mutation (Q415P) failed to generate this elaborate pattern in ~90% of the transfected cells (Fig. 7C and D). Instead, cells transfected with the Q415P construct showed a fine, punctate, incongruent pattern, which we described previously for pathogenic syndromic variants (33,36). However, cells transfected with any of the four nsCL/P variants were able to form this elaborate pattern to near-WT levels—between 70 and 80% (Fig. 7D). Thus, we concluded that the kinetics of microtubule association is not affected by these nsCL/P variants.

Next, we evaluated the levels of acetylation among these SPECC1L-associated microtubules (Fig. 7E–G). To minimize variability, we only assayed cells with elaborate microtubule pattern in WT and all four variants. Interestingly, we found that ~95% of WT transfected cells showed strong or moderate microtubule acetylation just 8 h after transfection, while ~5% showed low acetylation (Fig. 7H). These results suggest that this phenomenon is a two-step process, wherein SPECC1L first associates with a subset of microtubules, and then facilitates microtubule acetylation. We then analyzed acetylation of

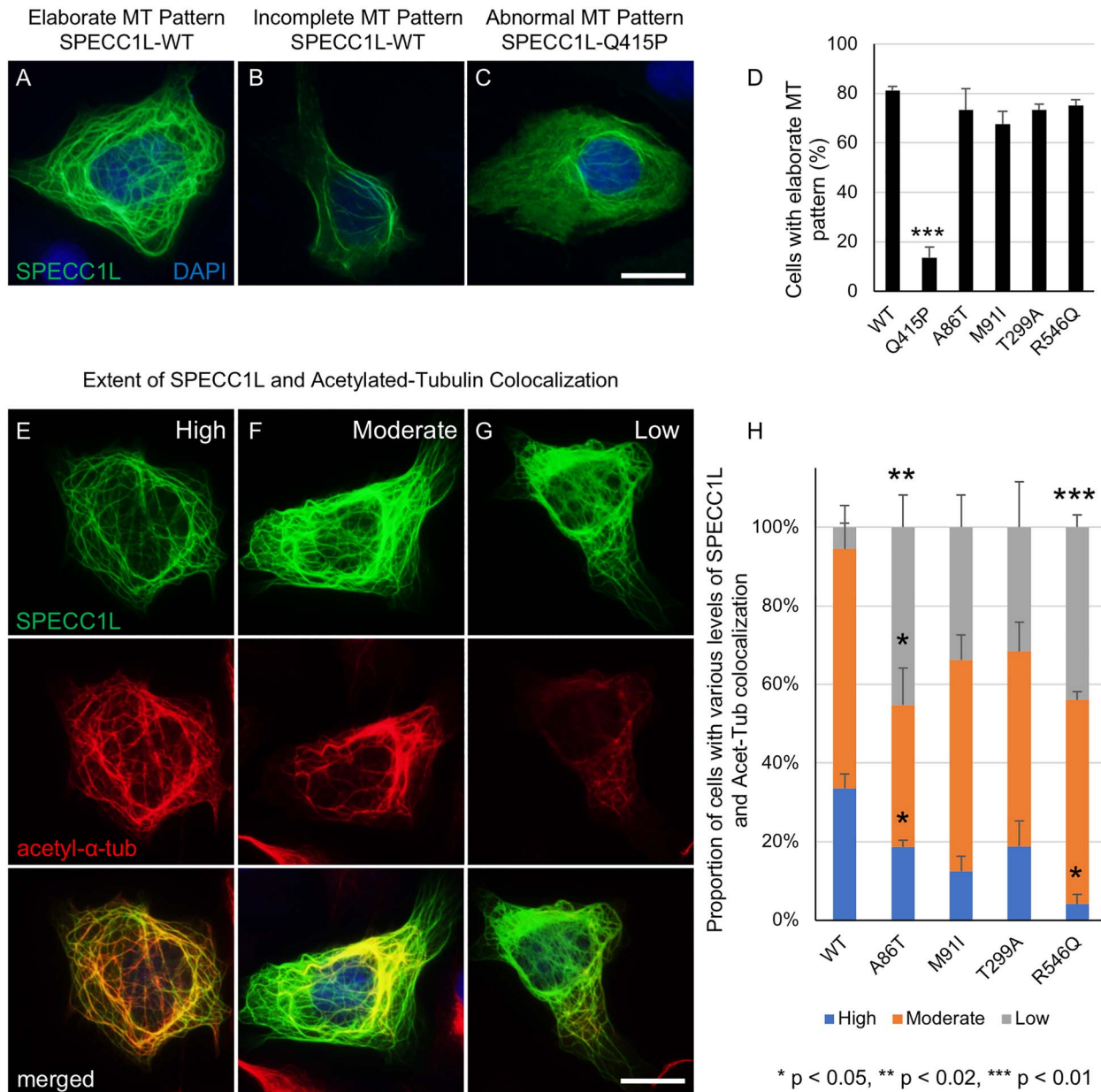


Figure 7. SPECC1L variants from non-syndromic patients result in reduced association with acetylated microtubules. (A–C) Representative images of U2OS cells transfected with WT (A and B) and Q415P (C) SPECC1L in U2OS cells. SPECC1L (green) was visualized by immunofluorescence and counterstained with DAPI (blue). (D) Transfected cells were scored for elaborate (A) or incomplete/abnormal microtubule patterning (B and C). The four variants identified in syndromic patients showed no changes, while the Q415P syndromic mutation resulted in a markedly reduced proportion of elaborate patterning. (E–G) Transfected cells were co-stained with SPECC1L (green) and acetylated- α -tubulin (red) and binned into high (E), moderate (F), or low (G) groups based on the extent of SPECC1L-associated acetylated tubulin staining. (H) Compared to wild-type, cells transfected with the A86T- and R546Q-SPECC1L constructs exhibited a significantly increased proportion of cells in the low group, and a significantly decreased proportion in the high (A86T, R546Q) and moderate (A86T) correlation groups. Scale bars are 20 μ m.

microtubules in cells expressing the nsCL/P variants 8 h after transfection. We found a statistically significant reduction in the number of highly acetylated microtubules, and a statistically significant increase in microtubules with low acetylation for the A86T and R546Q variants (Fig. 7H). The M91I and T299A variants did not show statistically significant differences from WT (Fig. 7H). It is possible that no significant change was identified in M91I samples because either the functional consequence on SPECC1L was too mild to be detected in our assay or it impacted SPECC1L function in a manner that did not alter microtubule acetylation. Compared to syndromic variants (Q415P) (33,36),

which fail to form the elaborate pattern, the two nsCL/P variants (A86T and R546Q) show a moderate reduction in SPECC1L function where they are able to associate with microtubules and form an elaborate pattern, but are delayed in subsequent acetylation of these microtubules.

Discussion

Rare SPECC1L variants were found in patients with atypical (33), syndromic (35,36) and now non-syndromic orofacial clefting. Interestingly—even with a small number of mutations

identified—SPECC1L variants from atypical and syndromic orofacial clefting patients cluster in the second coiled-coil and calponin homology domains. In contrast, the present variants from nsCL/P patients reside outside of these SPECC1L domains (Fig. 6). Functional analysis also indicates that the nsCL/P mutations are less severe than their syndromic counterparts (Fig. 7). As we better understand SPECC1L function at the molecular level, especially of the second coiled-coil domain, the functional differences between variants will become clearer.

We utilized a mouse model with a novel *Specc1l* truncation allele to confirm a role for SPECC1L in the regulation of palate development, consistent with the cleft palate phenotype observed in some patients with SPECC1L mutations (33,34,36). Our results show that palatal shelf elevation is particularly sensitive to *Specc1l* deficiency. While most *Specc1l*^{cGT/ΔC510} mutants eventually completed palatal shelf fusion, they all showed abnormalities in palate rugae pattern (Supplementary Material, Fig. S1), consistent with a palate-specific defect.

Palate elevation delays have been identified in several other mouse models (43–45,52,53). For instance, roughly half of *Fgfr2*^{C342Y/+} gain-of-function heterozygotes experience a delay in elevation, but only 4% penetrance of cleft palate (54). We propose that such delays represent a predisposing factor for cleft palate at birth, wherein a delay would result in cleft palate upon additional genetic or environmental insult. Thus, a delay in palatal shelf elevation represents a potential model for both the incomplete cleft palate penetrance that is frequently observed in syndromic CL/P (6,8) and for the complex etiology of nsCL/P.

We have shown previously that SPECC1L affects cell adhesion (33,37) and cell migration (33). Adherens junction markers E-cadherin and β -catenin, as well as F-actin, show increased expression upon SPECC1L deficiency *in vitro* and *in vivo* (37). Consistently, E-cadherin expression is decreased upon ectopic IRF6 expression (55). In the *Specc1l*^{cGT/ΔC510} mutants, we again see a general increase in F-actin staining. Importantly, β -catenin is mislocalized to the apical surface of the periderm cells in regions where the palatal shelf epithelium interfaces with both the tongue and buccal region. Such ectopic localization of adherens junction molecules has previously been shown in the periderm of *Irf6* mutants (29), suggesting that transient oral adhesions can slow palatal shelf elevation due to increased ‘friction’.

IRF6 mutations result in Van der Woude (1/35 000) and Popliteal Pterygium (1/300 000) syndromes. Several studies have also associated common IRF6 variants with nsCL/P at large (15,19,20). One of these variants is located in an upstream enhancer element of IRF6 (19) and affects IRF6 expression levels (56), and it is also associated with the severity of nsCL/P (57). We now show that SPECC1L expression in the palate epithelium and mesenchyme is dependent upon IRF6, thereby expanding the IRF6 network. However, since transgenic *Irf6* expression in the oral epithelium of *Irf6* mutants results in increased SPECC1L expression in the mesenchyme as well (Fig. 5C), it suggests that *Irf6* has a non-cell-autonomous role in the regulation of SPECC1L. *Irf6* has been shown previously to non-cell-autonomously regulate genes (58,59). It is currently unclear whether this non-cell autonomous regulation of SPECC1L is at the mRNA level, or rather a result of the disrupted cytoskeletal elements present in *Irf6* mutants (47,58). In the future, it would be interesting to explore expression levels of SPECC1L in mouse mutants for other genes known to interact with *Irf6*, including *Grhl3* (14), *Tfap2a* (60,61) and *Spry4* (60). In conclusion, our data suggest SPECC1L is a downstream cytoskeletal effector molecule in the palate, regulated by IRF6 transcription factor.

Materials and Methods

Patient information

For nsCL/P samples (Fig. 6), the study was approved by the ethical committee or by the Institutional Review Boards at all the participating sites in Ethiopia, Iowa, Nigeria and Philippines in accordance with the relevant guidelines and regulations. Study participants gave written informed consent for participation in this study in accordance with the Declaration of Helsinki and for the publication of this study. We also have adhered to standard biosecurity and institutional safety procedures in this study. Parent samples were not available for the six nsCL/P individuals identified with SPECC1L variants, therefore, we could not determine if these variants were inherited or *de novo*.

At Mayo Clinic (Rochester, MN), a second patient with SPECC1L p.Arg546Gln (c.1637G>A; Hg19/37) variant was identified with cleft lip and palate as well as hypertelorism, left eye vision loss, mild conductive hearing loss, gastroesophageal reflux disease, hypotonia, abnormal striae, kyphosis, small hand joint laxity, umbilical hernia, syncope, chronic pain, migraines, and mild motor, speech and developmental delay. She is primarily of Caucasian/European descent. The p.Arg546Gln variant was identified through clinical whole exome sequencing at Mayo Clinic Laboratories. This variant was paternally inherited; however, her father appears unaffected. She also carries a *de novo* 909 kb duplication involving the *OTX2* and *TMEM260* genes (arr[hg19] 14q22.3(56 702 987-57 611 978) × 3). This copy number variant was identified through clinical chromosomal microarray testing also performed at Mayo Clinic Laboratories.

Generation of *Specc1l*^{ΔC510} truncation allele

A ZFN was targeted to exon 4 of *mSpecc1l* near the exon 4/intron 4 boundary. 0.25 ng of targeting primer was co-injected with the ZFN expression construct into FVB/C57BL6/J hybrid blastocysts at the University of Kansas Medical Center Transgenic Facility. The injected embryos were transplanted into pseudo-pregnant females. The resulting progeny were analyzed by PCR for genomic deletions. A founder animal carrying one or more deletions was outbred with WT C57BL6/J females to establish a line. *Specc1l*^{ΔC510} was identified in such a manner. The deletion is 154 bp in length and spans the *mSpecc1l* exon 4/intron 4 boundary (NM_153406.3:c.1825_1941+37del). RT-PCR and western blot analyses were performed to determine the functional consequences of this genomic deletion. Primer sequences can be found in the Supplementary Material, Table S1).

Generation of *Specc1l*^{cGT} gene-trap allele

This strategy for generating a multifunctional gene-trap targeting construct has been described previously (Supplementary Material, Table S2) (41,62). In brief, 5' and 3' genomic homology regions (HRs) from the second intron of *Specc1l* were PCR-amplified from genomic DNA isolated from EDJ#22 (ATCC SCRC-1021) mouse 129S5/SvEvTac embryonic stem cells and cloned into pENTR-5'HR and pENTR-3'HR Entry clones. The three entry clones, pENTR-5'HR, pENTR-3'HR and prsFlipROSA β geo*TT0-ENTR11, and the pPNT-DEST-R4-R3 destination vector described previously (41) were combined to create the final ~20 kb targeted trapping vector, prsFlipROSA β geo*-*Specc1l*lin2, via the *in vitro* Multisite GATEWAY recombination system using LR Recombinase II Plus enzyme following manufacturer's

protocols (Thermo Fisher Scientific). Linearized plasmid DNA was electroporated into EDJ#22 ES cells. Positive ES colonies were selected first by Neomycin resistance using G418 (250 µg/ml) and then by RT-PCR for *Specc11-βgeo** fusion gene-trap transcript. Correctly targeted ES cells were microinjected into C57BL6/J blastocysts (KUMC Transgenic and Gene-Targeting Institutional Facility, Kansas City, KS). Chimeras were crossed to C57BL6/J mice for germline transmission. Heterozygous progeny was confirmed by PCR genotyping to identify the *Specc11^{CGT}* allele. All animal studies were performed consistent with protocols approved by the KUMC Institutional Animal Care and Use Committees.

Embryo processing and histological analysis

Mating pairs were set up in timed-matings and then checked for plugs on the following morning. Noon on that day, the plug was identified and is classified as embryonic day 0.5 (E0.5). At the given embryonic time-point, females were euthanized using a primary and a secondary method as approved by the institutional IACUC. Embryos were then harvested, washed in 1× PBS, imaged and fixed overnight in 4% paraformaldehyde at 4°C. For whole mount 4,6-diamidino-2-phenylindole (DAPI) imaging, the jaws of fixed embryo heads were removed and the exposed palates were then submerged in 500 nM DAPI dilactate overnight at 4°C, followed by imaging. For paraffin sectioning, embryos were gradually dehydrated in increasing concentrations of ethanol and processed for paraffin embedding using the Leica ASP300 tissue processor. For cryosectioning, embryos were submerged in 30% sucrose until the tissue sank, embedded in OCT solution and stored at –80°C until use. Sections were obtained between 8 and 10 µm. Brightfield and DAPI whole mount images were captured using a Nikon SMZ 1500 stereomicroscope. H&E paraffin histology images were captured on a Nikon Eclipse 80i upright microscope.

Immunostaining analysis

For the U2OS transfection experiments, coverslips were fixed with ice cold 4% paraformaldehyde for 10 min, permeabilized with 0.5% Triton X-100 in 1× PBS for 10 min, washed and then blocked in 10% normal goat serum (Thermo Fisher Scientific, 50062Z) for 1 h at room temperature. The primary antibody was incubated overnight at 4°C, washed in 1× PBS, then incubated in secondary antibody for 1 h at room temperature covered from light. Finally, the coverslips were washed again in 1× PBS and mounted on slides with Prolong Gold with DAPI (Invitrogen, P36930).

For immunostaining on embryo sections, conditions varied depending on the antibody used. Briefly, antigen retrieval was performed by heating the slides in sodium citrate buffer (10 mM Sodium Citrate, 0.05% Tween 20, pH 6.0) at 96°C for 10 min. The slides were then washed in H₂O, permeabilized with 0.5% Triton X-100 in 1× PBS for 30 min, washed in PBS, then blocked in 10% normal goat serum. Primary and secondary antibodies were incubated as described above. For phalloidin staining, antigen retrieval was not used, and the stain was included during secondary antibody incubation. Confocal images were captured on a Nikon A1R confocal laser microscope.

Primary antibodies: SPECC1L C-terminus (33), SPECC1L N-terminus (Proteintech, 25 390-1-AP), acetylated- α -tubulin (Sigma, T6793), Δ Np63 (Biolegend, 619001), β -catenin (Cell Signaling Technology, 2677), KI-67 (Cell Signaling Technology, 12202).

Secondary antibodies and stains: Goat anti-Rabbit IgG (H+L) Alexa 488 and 594 (Invitrogen; A-11008, A-11012), Goat anti-Mouse IgG1 Alexa 488 (Invitrogen, A-21121), Goat anti-Mouse IgG2a Alexa 594 (Invitrogen, A-21135), Goat anti-Mouse IgG3 Alexa 594 (Invitrogen; A-21155), Acti-stain 555 phalloidin (Cytoskeleton, PHDH1-A).

Quantification of periderm cells with abnormal expression pattern

Confocal Z-stacks of coronal sections stained by immunofluorescence were captured on a Nikon A1R confocal laser microscope. Periderm cells along the buccal and lingual interfaces of the palatal shelves were manually scored either as normal (no apical expression) or abnormal (apical expression). Cells were only scored if they could be classified as a periderm cell (flattened nucleus and/or Np63-negative) and if their boundaries were clearly identifiable by scanning through the Z-stack.

Western blot analysis

Protein extraction was performed by sonicating flash-frozen embryonic tissue in radioimmunoprecipitation assay buffer with HALT protease inhibitor Cocktail (Thermo Scientific, 78440). Samples were then spun down for 10 min at 13 000 rcf and the supernatant collected. Lysates were then electrophoresed in 4–15% gradient Mini-Protean TGX Stain-Free precast gels (Bio-RAD, #4568084) and transferred onto Immobilon PVDF (polyvinylidene difluoride) membranes (EMD Millipore, IPVH00010). PVDF membranes were then blocked in Odyssey Blocking Buffer (Li-Cor, 927-5000) either overnight at 4°C or at room temperature for 1 h. Primary antibodies used were anti-N-SPECC1L (1:2000; Proteintech, 25 390-1-AP) and anti-IRF6 (1:2000; Sigma, SAB2102995). The secondary antibody used was HRP-linked goat anti-rabbit IgG (1:10000; Cell Signaling Technologies). Femto SuperSignal West ECL reagent (Thermo Scientific, 34095) was used to develop the signal. Image Lab software (Bio-Rad) was used for quantitative analysis of the western blots.

Cell culture and transfection analysis

Human U2OS osteosarcoma cells (ATCC, HTB-96) were cultured in DMEM media with high glucose and pyruvate, supplemented with 10% fetal bovine serum and penicillin/streptomycin. U2OS cells were transfected with either WT SPECC1L-expressing construct (33) or with constructs carrying the Q415P (33), A86T, M91I, T299A and R546Q variants (present study). The GFP tag from previous studies (33) was removed in favor of visualizing the overexpressed protein by immunofluorescence. Transfected cells were analyzed for qualitative differences in the ability of SPECC1L to associate with microtubules and the extent of acetylation of associated microtubules (33,36).

Supplementary Material

Supplementary Material is available at HMG online.

Funding

National Institutes of Health (DE026172 to I.S., DE022378 to A.B., GM102801 to A.C., F31DE027284 to E.H.); Robert Wood Johnson Foundation (72429); JSPS KAKENHI (JP24249092, JP26861757,

JP17K11863); Center of Biomedical Research Excellence (COBRE) (National Institute of General Medical Sciences P20 GM104936); Kansas IDeA Network for Biomedical Research Excellence (National Institute of General Medical Sciences P20 GM103418); Kansas Intellectual and Developmental Disabilities Research Center (KIDDRC) (U54 Eunice Kennedy Shriver National Institute of Child Health and Human Development, HD 090216); the Confocal Imaging Facility, the Integrated Imaging Core, and the Transgenic and Gene Targeting Institutional Facility at the University of Kansas Medical Center are supported, in part, by NIH/NIGMS COBRE (P30GM122731) and by NIH/NICHD KIDDRC (U54HD090216).

Author Contributions

E.G.H., L.W.W. and I.S. conceived and designed the experiments. E.G.H., L.W.W., N.R.W., S.U., J.S., E.A.A., Y.K., D.S.A., J.P.G., L.P., S.Y., T.B. and B.C.B. performed the experiments. M.I., A.M., W.L.A., M.A.E., S.S., J.C.M. and A.B. provided nsCLP samples and SPECC1L sequencing data. L.E.S., D.B. and S.A.K. provided the clinical and sequence data on the second patient with p.Arg546Gln variant. E.G.H., L.W.W., N.R.W., S.U., J.S., Y.K., T.B., B.C.B., B.C.S., A.B. and I.S. analyzed the data. E.G.H. and I.S. wrote the paper. J.K., B.C.B., B.C.S. and A.B. edited the manuscript. All authors reviewed the manuscript.

Conflict of Interest statement

The authors do not have any competing financial interests pertaining to the studies presented here.

Acknowledgements

The authors would like to acknowledge the Genome Aggregation Database (gnomAD) and its contributors (<https://gnomad.broadinstitute.org/about>).

References

- Rahimov, F., Jugessur, A. and Murray, J.C. (2012) Genetics of nonsyndromic orofacial clefts. *Cleft Palate Craniofac. J.*, **49**, 73–91.
- Mossey, P.A. and Modell, B. (2012) Epidemiology of oral clefts 2012: an international perspective. *Front. Oral Biol.*, **16**, 1–18.
- Stanier, P. and Moore, G.E. (2004) Genetics of cleft lip and palate: syndromic genes contribute to the incidence of non-syndromic clefts. *Hum. Mol. Genet.*, **13**(Spec no. 1), R73–R81.
- Leslie, E.J. and Marazita, M.L. (2013) Genetics of cleft lip and cleft palate. *Am. J. Med. Genet. C*, **163C**, 246–258.
- Murray, J.C. (1995) Face facts: genes, environment, and clefts. *Am. J. Hum. Genet.*, **57**, 227–232.
- Jugessur, A., Farlie, P.G. and Kilpatrick, N. (2009) The genetics of isolated orofacial clefts: from genotypes to subphenotypes. *Oral Dis.*, **15**, 437–453.
- Pengelly, R.J., Arias, L., Martinez, J., Upstill-Goddard, R., Seaby, E.G., Gibson, J., Ennis, S., Collins, A. and Briceno, I. (2016) Deleterious coding variants in multi-case families with non-syndromic cleft lip and/or palate phenotypes. *Sci. Rep.*, **6**, 30457.
- Dixon, M.J., Marazita, M.L., Beaty, T.H. and Murray, J.C. (2011) Cleft lip and palate: understanding genetic and environmental influences. *Nat. Rev. Genet.*, **12**, 167–178.
- Marazita, M.L. (2012) The evolution of human genetic studies of cleft lip and cleft palate. *Annu. Rev. Genomics Hum. Genet.*, **13**, 263–283.
- Adeyemo, W.L. and Butali, A. (2017) Genetics and genomics etiology of nonsyndromic orofacial clefts. *Mol. Genet. Genomic Med.*, **5**, 3–7.
- Kondo, S., Schutte, B.C., Richardson, R.J., Bjork, B.C., Knight, A.S., Watanabe, Y., Howard, E., de Lima, R.L., Daack-Hirsch, S., Sander, A. et al. (2002) Mutations in IRF6 cause Van der Woude and popliteal pterygium syndromes. *Nat. Genet.*, **32**, 285–289.
- Kousa, Y.A. and Schutte, B.C. (2016) Toward an orofacial gene regulatory network. *Dev. Dyn.*, **245**, 220–232.
- Leslie, E.J., Standley, J., Compton, J., Bale, S., Schutte, B.C. and Murray, J.C. (2013) Comparative analysis of IRF6 variants in families with Van der Woude syndrome and popliteal pterygium syndrome using public whole-exome databases. *Genet. Med.*, **15**, 338–344.
- Peyrard-Janvid, M., Leslie, E.J., Kousa, Y.A., Smith, T.L., Dunnwald, M., Magnusson, M., Lentz, B.A., Unneberg, P., Fransson, I., Koillinen, H.K. et al. (2014) Dominant mutations in GRHL3 cause Van der Woude syndrome and disrupt oral periderm development. *Am. J. Hum. Genet.*, **94**, 23–32.
- Beaty, T.H., Murray, J.C., Marazita, M.L., Munger, R.G., Ruczinski, I., Hetmanski, J.B., Liang, K.Y., Wu, T., Murray, T., Fallin, M.D. et al. (2010) A genome-wide association study of cleft lip with and without cleft palate identifies risk variants near MAFB and ABCA4. *Nat. Genet.*, **42**, 525–529.
- Gowans, L.J., Busch, T.D., Mossey, P.A., Eshete, M.A., Adeyemo, W.L., Aregbesola, B., Donkor, P., Arthur, F.K., Agbenorku, P., Olutayo, J. et al. (2017) The prevalence, penetrance, and expressivity of etiologic IRF6 variants in orofacial clefts patients from sub-Saharan Africa. *Mol. Genet. Genomic Med.*, **5**, 164–171.
- Leslie, E.J., Koboldt, D.C., Kang, C.J., Ma, L., Hecht, J.T., Wehby, G.L., Christensen, K., Czeizel, A.E., Deleyiannis, F.W., Fulton, R.S. et al. (2016) IRF6 mutation screening in non-syndromic orofacial clefting: analysis of 1521 families. *Clin. Genet.*, **90**, 28–34.
- Leslie, E.J., Liu, H., Carlson, J.C., Shaffer, J.R., Feingold, E., Wehby, G., Laurie, C.A., Jain, D., Laurie, C.C., Doheny, K.F. et al. (2016) A genome-wide association study of nonsyndromic cleft palate identifies an etiologic missense variant in GRHL3. *Am. J. Hum. Genet.*, **98**, 744–754.
- Rahimov, F., Marazita, M.L., Visel, A., Cooper, M.E., Hitchler, M.J., Rubini, M., Domann, F.E., Govil, M., Christensen, K., Bille, C. et al. (2008) Disruption of an AP-2alpha binding site in an IRF6 enhancer is associated with cleft lip. *Nat. Genet.*, **40**, 1341–1347.
- Zuccherro, T.M., Cooper, M.E., Maher, B.S., Daack-Hirsch, S., Nepomuceno, B., Ribeiro, L., Caprau, D., Christensen, K., Suzuki, Y., Machida, J. et al. (2004) Interferon regulatory factor 6 (IRF6) gene variants and the risk of isolated cleft lip or palate. *N. Engl. J. Med.*, **351**, 769–780.
- Botti, E., Spallone, G., Moretti, F., Marinari, B., Pinetti, V., Galanti, S., De Meo, P.D., De Nicola, F., Ganci, F., Castrignano, T. et al. (2011) Developmental factor IRF6 exhibits tumor suppressor activity in squamous cell carcinomas. *Proc. Nat. Acad. Sci. U.S.A.*, **108**, 13710–13715.
- de la Garza, G., Schleiffarth, J.R., Dunnwald, M., Mankad, A., Weirather, J.L., Bonde, G., Butcher, S., Mansour, T.A., Kousa, Y.A., Fukazawa, C.F. et al. (2013) Interferon regulatory factor 6 promotes differentiation of the periderm by activating

- expression of Grainyhead-like 3. *J. Invest. Dermatol.*, **133**, 68–77.
23. Ingraham, C.R., Kinoshita, A., Kondo, S., Yang, B., Sajan, S., Trout, K.J., Malik, M.I., Dunnwald, M., Goudy, S.L., Lovett, M. et al. (2006) Abnormal skin, limb and craniofacial morphogenesis in mice deficient for interferon regulatory factor 6 (Irf6). *Nat. Genet.*, **38**, 1335–1340.
 24. Richardson, R.J., Dixon, J., Malhotra, S., Hardman, M.J., Knowles, L., Boot-Handford, R.P., Shore, P., Whitmarsh, A. and Dixon, M.J. (2006) Irf6 is a key determinant of the keratinocyte proliferation-differentiation switch. *Nat. Genet.*, **38**, 1329–1334.
 25. Leslie, E.J., Mansilla, M.A., Biggs, L.C., Schuette, K., Bullard, S., Cooper, M., Dunnwald, M., Lidral, A.C., Marazita, M.L., Beaty, T.H. et al. (2012) Expression and mutation analyses implicate ARHGAP29 as the etiologic gene for the cleft lip with or without cleft palate locus identified by genome-wide association on chromosome 1p22. *Birth Defects Res. A Clin. Mol. Teratol.*, **94**, 934–942.
 26. Letra, A., Maili, L., Mulliken, J.B., Buchanan, E., Blanton, S.H. and Hecht, J.T. (2014) Further evidence suggesting a role for variation in ARHGAP29 variants in nonsyndromic cleft lip/palate. *Birth Defects Res. A Clin. Mol. Teratol.*, **100**, 679–685.
 27. Savastano, C.P., Brito, L.A., Faria, A.C., Seto-Salvia, N., Peskett, E., Musso, C.M., Alvizi, L., Ezquina, S.A., James, C., Gosgene et al. (2017) Impact of rare variants in ARHGAP29 to the etiology of oral clefts: role of loss-of-function vs missense variants. *Clin. Genet.*, **91**, 683–689.
 28. Liu, H., Busch, T., Eliason, S., Anand, D., Bullard, S., Gowans, L.J.J., Nidey, N., Petrin, A., Augustine-Akpan, E.A., Saadi, I. et al. (2017) Exome sequencing provides additional evidence for the involvement of ARHGAP29 in Mendelian orofacial clefting and extends the phenotypic spectrum to isolated cleft palate. *Birth Defects Res. A Clin. Mol. Teratol.*, **109**, 27–37.
 29. Richardson, R.J., Dixon, J., Jiang, R. and Dixon, M.J. (2009) Integration of IRF6 and Jagged2 signalling is essential for controlling palatal adhesion and fusion competence. *Hum. Mol. Genet.*, **18**, 2632–2642.
 30. Richardson, R.J., Hammond, N.L., Coulombe, P.A., Saloranta, C., Nousiainen, H.O., Salonen, R., Berry, A., Hanley, N., Headon, D., Karikoski, R. et al. (2014) Periderm prevents pathological epithelial adhesions during embryogenesis. *J. Clin. Invest.*, **124**, 3891–3900.
 31. Lan, Y., Xu, J. and Jiang, R. (2015) Cellular and molecular mechanisms of palatogenesis. *Curr. Top. Dev. Biol.*, **115**, 59–84.
 32. Paul, B.J., Palmer, K., Sharp, J.C., Pratt, C.H., Murray, S.A. and Dunnwald, M. (2017) ARHGAP29 mutation is associated with abnormal oral epithelial adhesions. *J. Dent. Res.*, **96**, 1298–1305.
 33. Saadi, I., Alkuraya, F.S., Gisselbrecht, S.S., Goessling, W., Cavallesco, R., Turbe-Doan, A., Petrin, A.L., Harris, J., Siddiqui, U., Grix, A.W., Jr. et al. (2011) Deficiency of the cytoskeletal protein SPECC1L leads to oblique facial clefting. *Am. J. Hum. Genet.*, **89**, 44–55.
 34. Bhoj, E.J., Haye, D., Toutain, A., Bonneau, D., Nielsen, I.K., Lund, I.B., Bogaard, P., Leenskjold, S., Karaer, K., Wild, K.T. et al. (2019) Phenotypic spectrum associated with SPECC1L pathogenic variants: new families and critical review of the nosology of Teebi, Opitz GBBB, and Baraitser-Winter syndromes. *Eur. J. Med. Genet.*, **62**(12):103588. Epub 2018 Nov 22.
 35. Bhoj, E.J., Li, D., Harr, M.H., Tian, L., Wang, T., Zhao, Y., Qiu, H., Kim, C., Hoffman, J.D., Hakonarson, H. et al. (2015) Expanding the SPECC1L mutation phenotypic spectrum to include Teebi hypertelorism syndrome. *Am. J. Med. Genet. A*, **167A**, 2497–2502.
 36. Kruszka, P., Li, D., Harr, M.H., Wilson, N.R., Swarr, D., McCormick, E.M., Chiavacci, R.M., Li, M., Martinez, A.F., Hart, R.A. et al. (2015) Mutations in SPECC1L, encoding sperm antigen with calponin homology and coiled-coil domains 1-like, are found in some cases of autosomal dominant Opitz G/BBB syndrome. *J. Med. Genet.*, **52**, 104–110.
 37. Wilson, N.R., Olm-Shipman, A.J., Acevedo, D.S., Palaniyandi, K., Hall, E.G., Kosa, E., Stumpff, K.M., Smith, G.J., Pitstick, L., Liao, E.C. et al. (2016) SPECC1L deficiency results in increased adherens junction stability and reduced cranial neural crest cell delamination. *Sci. Rep.*, **6**, 17735.
 38. Trainor, P.A. (2010) Craniofacial birth defects: the role of neural crest cells in the etiology and pathogenesis of Treacher Collins syndrome and the potential for prevention. *Am. J. Med. Genet. A*, **152A**, 2984–2994.
 39. Snider, T.N. and Mishina, Y. (2014) Cranial neural crest cell contribution to craniofacial formation, pathology, and future directions in tissue engineering. *Birth Defects Res. C*, **102**, 324–332.
 40. Turgeon, B. and Meloche, S. (2009) Interpreting neonatal lethal phenotypes in mouse mutants: insights into gene function and human diseases. *Physiol. Rev.*, **89**, 1–26.
 41. Strassman, A., Schnutgen, F., Dai, Q., Jones, J.C., Gomez, A.C., Pitstick, L., Holton, N.E., Moskal, R., Leslie, E.R., von Melchner, H. et al. (2017) Generation of a multipurpose Prdm16 mouse allele by targeted gene trapping. *Dis. Model Mech.*, **10**, 909–922.
 42. Schnutgen, F., De-Zolt, S., Van Sloun, P., Hollatz, M., Floss, T., Hansen, J., Altschmied, J., Seisenberger, C., Ghyselinck, N.B., Ruiz, P. et al. (2005) Genomewide production of multipurpose alleles for the functional analysis of the mouse genome. *Proc. Nat. Acad. Sci. U.S.A.*, **102**, 7221–7226.
 43. Gritli-Linde, A. (2008) The etiopathogenesis of cleft lip and cleft palate: usefulness and caveats of mouse models. *Curr. Top. Dev. Biol.*, **84**, 37–138.
 44. Gritli-Linde, A. (2007) Molecular control of secondary palate development. *Dev. Biol.*, **301**, 309–326.
 45. Bush, J.O. and Jiang, R. (2012) Palatogenesis: morphogenetic and molecular mechanisms of secondary palate development. *Development*, **139**, 231–243.
 46. Casey, L.M., Lan, Y., Cho, E.S., Maltby, K.M., Gridley, T. and Jiang, R. (2006) Jag2-Notch1 signaling regulates oral epithelial differentiation and palate development. *Dev. Dyn.*, **235**, 1830–1844.
 47. Biggs, L.C., Naridze, R.L., DeMali, K.A., Lusche, D.F., Kuhl, S., Soll, D.R., Schutte, B.C. and Dunnwald, M. (2014) Interferon regulatory factor 6 regulates keratinocyte migration. *J. Cell Sci.*, **127**, 2840–2848.
 48. Kousa, Y.A., Moussa, D. and Schutte, B.C. (2017) IRF6 expression in basal epithelium partially rescues Irf6 knockout mice. *Dev. Dyn.*, **246**, 670–681.
 49. Lek, M., Karczewski, K.J., Minikel, E.V., Samocha, K.E., Banks, E., Fennell, T., O'Donnell-Luria, A.H., Ware, J.S., Hill, A.J., Cummings, B.B. et al. (2016) Analysis of protein-coding genetic variation in 60,706 humans. *Nature*, **536**, 285–291.
 50. TogoVar [https://togovar.biosciencedbc.jp] Japan Science and Technology Agency (Japan) (2018). National Bioscience Database Center Tokyo.
 51. Zielinski, D., Markus, B., Sheikh, M., Gymrek, M., Chu, C., Zaks, M., Srinivasan, B., Hoffman, J.D., Aizenbud, D. and Erlich, Y. (2014) OTX2 duplication is implicated in hemifacial microsomia. *PLoS One*, **9**, e96788.

52. Funato, N., Nakamura, M. and Yanagisawa, H. (2015) Molecular basis of cleft palates in mice. *World J. Biol. Chem.*, **6**, 121–138.
53. Li, C., Lan, Y., Krumlauf, R. and Jiang, R. (2017) Modulating Wnt Signaling rescues palate morphogenesis in Pax9 mutant mice. *J. Dent. Res.*, **96**, 1273–1281.
54. Snyder-Warwick, A.K., Perlyn, C.A., Pan, J., Yu, K., Zhang, L. and Ornitz, D.M. (2010) Analysis of a gain-of-function FGFR2 Crouzon mutation provides evidence of loss of function activity in the etiology of cleft palate. *Proc. Nat. Acad. Sci. U.S.A.*, **107**, 2515–2520.
55. Ke, C.Y., Xiao, W.L., Chen, C.M., Lo, L.J. and Wong, F.H. (2015) IRF6 is the mediator of TGFbeta3 during regulation of the epithelial mesenchymal transition and palatal fusion. *Sci. Rep.*, **5**, 12791.
56. Fakhouri, W.D., Rhea, L., Du, T., Sweezer, E., Morrison, H., Fitzpatrick, D., Yang, B., Dunnwald, M. and Schutte, B.C. (2012) MCS9.7 enhancer activity is highly, but not completely, associated with expression of Irf6 and p63. *Dev. Dyn.*, **241**, 340–349.
57. Kerameddin, S., Namipashaki, A., Ebrahimi, S. and Ansari-Pour, N. (2015) IRF6 is a marker of severity in nonsyndromic cleft lip/palate. *J. Dent. Res.*, **94**, 226S–232S.
58. Goudy, S., Angel, P., Jacobs, B., Hill, C., Mainini, V., Smith, A.L., Kousa, Y.A., Caprioli, R., Prince, L.S., Baldwin, S. et al. (2013) Cell-autonomous and non-cell-autonomous roles for IRF6 during development of the tongue. *PLoS One*, **8**, e56270.
59. Fakhouri, W.D., Metwalli, K., Naji, A., Bakhiet, S., Quispesalcedo, A., Nitschke, L., Kousa, Y.A. and Schutte, B.C. (2017) Intercellular genetic interaction between Irf6 and Twist1 during craniofacial development. *Sci. Rep.*, **7**, 7129.
60. Kousa, Y.A., Roushangar, R., Patel, N., Walter, A., Marangoni, P., Krumlauf, R., Klein, O.D. and Schutte, B.C. (2017) IRF6 and SPRY4 signaling interact in periderm development. *J. Dent. Res.*, **96**, 1306–1313.
61. Kousa, Y.A., Zhu, H., Fakhouri, W.D., Lei, Y., Kinoshita, A., Roushangar, R.R., Patel, N.K., Agopian, A.J., Yang, W., Leslie, E.J. et al. (2019) The TFAP2A-IRF6-GRHL3 genetic pathway is conserved in neurulation. *Hum. Mol. Genet.*, **28**, 1726–1737.
62. Nagy, A., Gertsenstein, M., Vintersten, K. and Behringer, R. (2003) *Manipulating the Mouse Embryo: A Laboratory Manual*. Cold Spring Harbor Laboratory Press Cold Spring Harbor.
63. Adzhubei, I.A., Schmidt, S., Peshkin, L., Ramensky, V.E., Gerasimova, A., Bork, P., Kondrashov, A.S. and Sunyaev, S.R. (2010) A method and server for predicting damaging missense mutations. *Nat. Meth.*, **7**, 248–249.
64. Sim, N.L., Kumar, P., Hu, J., Henikoff, S., Schneider, G. and Ng, P.C. (2012) SIFT web server: predicting effects of amino acid substitutions on proteins. *Nucleic Acids Res.*, **40**, W452–W457.